AIAA JOURNAL
Vol. 38, No. 10, October 2000

Surface Pressure Fluctuations Beneath Two- and Three-Dimensional Turbulent Boundary Layers

Michael C. Goody* and Roger L. Simpson†
Virginia Polytechnic Institute and State University, Blacksburg, Virginia 24061-0203

Surface pressure fluctuation measurements were made in two-dimensional turbulent boundary layers at two Reynolds numbers ($Re_\theta = 7.3 \times 10^3$ and 2.34×10^4) and pressure-driven three-dimensional turbulent boundary layers at two Reynolds numbers (approach $Re_\theta = 5.94 \times 10^3$ and 2.32×10^4). The collapse of spectral levels at middle and high frequencies and the effects of inner and outer boundary-layer scaling variables are shown for a wide range of Reynolds numbers ($1.4 \times 10^3 < 2.34 \times 10^4$) for the two-dimensional flows. Such scaling parameters do not collapse the pressure spectra beneath three-dimensional flows, which have a nearly constant, or flat, midfrequency range, and at some measurement stations and spectral levels within the flat- and high-frequency spectral ranges that significantly raise p'. Additionally, dimensional spectral levels within the flat-frequency range are independent of Reynolds number. Analysis based on the Poisson equation shows that the variation of the high-frequency spectral levels is related to the variation in near-wall mean velocity gradients and $\overline{v^2}$ structure due to the spanwise pressure gradient.

Nomenclature

d	= pressure transducer sensing diameter
d^+	= $u_\tau d/\nu$, nondimensional
$\mathrm{d}\Omega$	= differential volume element
$\mathrm{d}\Omega^+$	= $\mathrm{d}\Omega u_\tau^3/\nu^3$, nondimensional
f	= frequency, Hz
k_1, k_3	= wave number vector components in the x and z directions, respectively
k_1^+, k_3^+	= $u_\tau k_1/\nu$ and $u_\tau k_3/\nu$, nondimensional
p	= pressure fluctuation at the surface (wall)
Q_e	= dynamic pressure at the edge of the boundary layer, $\frac{1}{2}\rho U_e^2$
Re_δ	= boundary-layer thickness Reynolds number, $u_\tau \delta/\nu$
Re_θ	= momentum thickness Reynolds number, $U_\infty \theta/\nu$
r_S	= distance between a point on the surface where pressure fluctuations are measured and the point in the flow that is the source of the pressure fluctuations
r_S^+	= $u_\tau r_S/\nu$, nondimensional
t	= time
$t_{\max}$	= maximum thickness of the wing, 7.17 cm
U, V, W	= mean velocity components in the x, y, and z directions, respectively
U_C	= magnitude of the convection velocity of pressure fluctuations
U_{C1}, U_{C3}	= convection velocity vector components in the x and z directions, respectively
U_e	= total velocity at edge of the boundary layer
U^+, V^+, W^+	= U/u_τ, V/u_τ, w/u_τ, respectively, nondimensional
U_∞	= wind-tunnel freestream velocity
u, v, w	= fluctuating velocity components in the x, y, and z directions, respectively
u_τ	= friction velocity, $(\tau_W/\rho)^{1/2}$
u^+, v^+, w^+	= u/u_τ, v/u_τ, and w/u_τ, respectively, nondimensional
v_ω	= amplitude of the v-fluctuating velocity component at a particular frequency
x	= streamwise coordinate
y	= wall-normal coordinate
y^+	= $u_\tau y/\nu$, nondimensional
z	= spanwise coordinate
β_{FS}	= freestream mean flow angle measured relative to the wind-tunnel centerline
β_W	= near-wall mean flow angle measured relative to the wind-tunnel centerline
Δ	= boundary-layer thickness based on the velocity defect law, $U_e\delta^*/u_\tau$
δ	= boundary-layer thickness; distance from the wall where $(U^2 + W^2)^{1/2}/U_e = 0.995$
δ^*	= boundary-layer magnitude displacement thickness, $\int_0^\infty \left(1 - \frac{\sqrt{U^2 + W^2}}{U_e}\right) \mathrm{d}y$
θ	= boundary-layer streamwise momentum thickness, $\int_0^\infty \left(1 - \frac{U}{U_e}\right)\frac{U}{U_e}\,\mathrm{d}y$
ν	= kinematic viscosity of air
ρ	= mass density of flow
τ_W	= shear-stress magnitude at the surface (wall)
Φ	= power spectrum of surface pressure fluctuations such that $\overline{p^2} = \int_0^\infty \Phi(\omega)\,\mathrm{d}\omega$
Φ_0	= $\Phi u_\tau/\tau_W^2\,\delta$, nondimensional
Φ^+	= $\Phi u_\tau^2/\tau_W^2\,\nu$, nondimensional
ω	= circular frequency, rad/s
ω_0	= $\omega\delta/u_\tau$, nondimensional
ω^+	= $\omega\nu/u_\tau^2$, nondimensional

Superscript

$'$	= root mean square value of a fluctuating quantity

Presented as Paper 99-0608 at the AIAA 37th Aerospace Sciences Meeting, Reno, NV, 11–14 January 1999; received 14 June 1999; revision received 2 February 2000; accepted for publication 4 February 2000.

*Graduate Assistant, Department of Aerospace and Ocean Engineering, 215 Randolph Hall. Student Member AIAA.

†Jack E. Cowling Professor, Department of Aerospace and Ocean Engineering, 215 Randolph Hall. Fellow AIAA.

I. Introduction

THE pressure fluctuations in a three-dimensional turbulent shear flow on a body are a source of noise and vibration. Though

common, the sources of p are not well understood and are difficult to model. An increased understanding of the physics of this flowfield may improve the calculation, and perhaps control, of the noise generated by undersea vehicles and the handling characteristics of aircraft at high angle of attack.

Most practical flows encountered in nature are three dimensional. Therefore, an understanding of the complex flow physics of three-dimensional flow are of practical engineering interest. The velocity field of each of the three-dimensional, pressure-driven flows of the present study is well documented for a wide range of Reynolds numbers. Detailed references are given by Ölçmen and Simpson,[1] Simpson,[2] and Fleming and Simpson.[3] Previous studies of the surface pressure fluctuations in the three-dimensional flow of the present study are confined to the highly unsteady flow near the wing–body junction in front of the nose of the wing. Rife et al.[4] examined the relationship between the bimodal velocity and surface pressure fluctuations and Ölçmen and Simpson[5] studied the effect of wing shape on surface pressure fluctuations in the nose region. The present study investigates p in the three-dimensional flow away from the wing–body junction.

Most fundamental experimental investigations of p beneath a turbulent boundary layer have been confined to equilibrium, or near-equilibrium, two-dimensional boundary layers.[6–8] In equilibrium boundary layers, velocity-profile similarity scales based on inner and outer boundary-layer variables have been shown to scale high- and low-frequency regions of the surface pressure spectrum, respectively.[9,10] Recent reviews of the scaling behavior of the pressure power spectrum have been done by Keith et al.[11] and Bull.[12] Some uncertainty in the measured behavior has been attributed to the observed Reynolds number dependence of p' (Refs. 6 and 10), the limited high-frequency response of transducers due to finite sensing area,[13–16] and the presence of pressure fluctuations due to nonturbulent sources, that is, external acoustic and vibration.[7,10,17]

Surface pressure fluctuations beneath a turbulent boundary layer are related to velocity fluctuations within the boundary layer through a Poisson-type differential equation.[18–20] The Poisson equation may be integrated and shows that surface pressure fluctuations are produced from large regions of the flow. However, the influence of a given source falls off as $1/r_S$.

Much analysis of surface pressure fluctuations beneath equilibrium, two-dimensional boundary layers exists in the literature; however, the same is not true for complex three-dimensional boundary layers. Panton[21] reformulated the two-dimensional spectral model of Witting[22] to three dimensions by converting frequency to phase velocity and assuming two distinct convection velocities: one for the inner boundary layer and another for the outer boundary layer. He concluded that the conversion from frequency to phase velocity and convection velocity was viable; however, a continuous function for the convection velocity across the boundary layer was likely required, rather than only two distinct values. More data, such as the present study, are needed to quantify features of surface pressure fluctuations that are unique to three-dimensional flows. Such data are directly related to the noise and vibration produced by practical three-dimensional flows.

II. Experimental Apparatus and Techniques

The measurements were made in the boundary-layer wind tunnel of the Aerospace and Ocean Engineering Department at Virginia Polytechnic Institute and State University. The tunnel has a 24-ft-long test section with a rectangular cross section that is 3 ft wide with variable height to adjust the streamwise freestream velocity. The nominal freestream air speed was 27.5 m/s for the two lower momentum thickness Reynolds number flows and 32.0 m/s for the two higher momentum thickness Reynolds number flows. All measurements were made at ambient pressure and a temperature of 25°C ± 1°C.

The pressure-driven, three-dimensional turbulent boundary layer was produced by a wing–body junction geometry. The wing used has a 3:2 elliptical nose, NACA 0020 tailed wing profile. It has a maximum thickness of 0.0717 m, a chord length of 0.305 m, and a height of 0.232 m. The wing was mounted at zero angle of attack with the leading edge 0.302 m downstream of the test section entrance in the $Re_\theta = 5.94 \times 10^3$ flow and 0.707 m downstream of the test section entrance in the $Re_\theta = 2.32 \times 10^4$ flow. A 0.0037-m gap was left between the ceiling of the test section and the top of the wing model to prevent the formation of a second horseshoe vortex. Measurements of p were made at 10 stations that traverse one side of the wing (Fig. 1) and are away from the wing–body junction horseshoe vortex. In Fig. 1 solid arrows are the wall-shear-stress direction in the $Re_\theta = 5.94 \times 10^3$ flow (β_W in Table 1). Open arrows are the freestream direction in the $Re_\theta = 5.94 \times 10^3$ flow (β_{FS} in Table 1). The y coordinate is normal to the paper, forming a right-handed coordinate system. The measurement stations were chosen based on the existence of previously reported mean velocity, Reynolds stress, triple products, and skin-friction measurements.[1,23–27] Some relevant flow parameters are given in Tables 1 and 2. The two-dimensional zero-pressure-gradient flows were produced by removing the wing. In the $Re_\theta = 7.3 \times 10^3$ flow, measurements were carried out 0.303 m downstream of the test section entrance. In the $Re_\theta = 2.34 \times 10^4$ flow, measurements were carried out 0.696 m downstream of the test section entrance. Streamwise traverses showed a closely constant freestream velocity (±2%) when the wing was removed.[25]

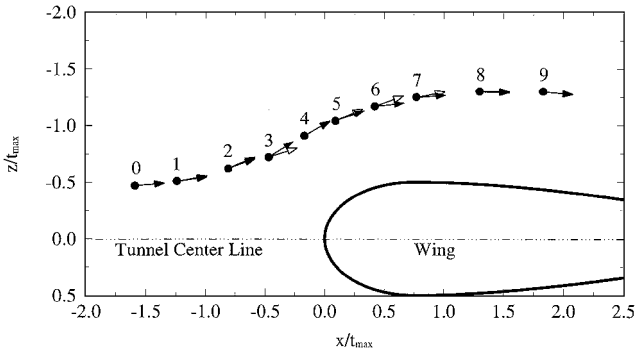

Fig. 1 Wing shape and measurement stations.

The pressure transducer was an Endevco model 8507-C2, which has a flat-frequency response from 0 to 70 kHz. The transducer signal was amplified by a Measurements Group Model 2310 strain gauge conditioning amplifier and stored to 12-bit precision by an IBM-type personal computer. The surface pressure fluctuations were sampled at 67 kHz. At each location, 512 records of 32,768 contiguous samples per record were acquired. The total sampling period at each measurement location was 16 min to ensure that all relevant timescales were measured. (A time interval was allowed to elapse in between the acquisition of each contiguous record of data to lengthen the total sample period. These time intervals were not necessarily equal to one another.)

Access to the flowfield was provided through a 5×10^{-4} m diam pinhole, which was used to decrease spatial averaging. The pinhole and associated dead volume have a second-order transfer function that is flat within the frequency range of interest here with a resonant frequency near 28 kHz. The sensitivity was calibrated by applying a known constant pressure to the pressure transducer and measuring the output voltage. The pinhole was used to increase spatial resolution; otherwise, contributions to the pressure fluctuation from sources that are smaller than the transducer sensing area would be spatially integrated and, thereby, attenuated. This effect has been investigated,[13–16] and Corcos[13] provides a correction to the wall pressure spectrum in terms of $\omega d/2U_C$, where ω/U_C is the wave number. Schewe[14] maintains that this correction is adequate for $\omega d/2U_C < 4$. Recently, Lueptow[15] reported similar results. In the present study, $\omega d/2U_C < 2.5$, assuming that $U_C = 14u_\tau$ (Ref. 28). Gravante et al.[16] asserted that the maximum allowable sensing diameter to avoid spectral attenuation at high frequencies is in the range $12 < d^+ < 18$, and for $d^+ < 27$ the reduction in p' was "barely observable."[16] In the present study, $26 < d^+ < 40$. To have $d^+ \leq 18$ here would require a pinhole diameter of 2.25×10^{-4} m, which in turn would lower the Helmholtz resonant frequency of the pinhole to 12.6 kHz. A resonant frequency of 12.6 kHz would significantly affect the measured high-frequency spectral values and, thus, offset any benefit of better spatial resolution.

Table 1 Some relevant boundary-layer parameters[a]

Station	U_e, m/s	$\delta^* \times 10^3$, m	Q_e, Pa	$\left[\frac{\partial C_p}{\partial(x/t_{max})}\right]_{WC}$	$\left[\frac{\partial C_p}{\partial(z/t_{max})}\right]_{WC}$	β_W, deg	β_{FS}, deg
			$Re_\theta = 7.3 \times 10^3$ (two-dimensional) and 5.94×10^3 (three-dimensional)[b]				
Two-dimensional	27.1	6.20	399	——	——	——	——
0	26.4	N/A	379	N/A	N/A	−6.1	−1.7
1	24.9	6.90	340	0.069	0.112	−11.5	−2.6
2	24.8	7.54	337	−0.054	0.208	−24.0	−4.8
3	25.3	6.86	351	−0.378	0.146	−33.7	−8.6
4	27.3	5.53	409	−0.449	−0.097	−30.6	−9.5
5	29.5	5.37	477	−0.416	−0.218	−19.7	−7.7
6	30.5	5.24	511	−0.287	−0.400	−7.2	−5.1
7	31.0	5.20	528	0.042	−0.480	−3.5	−2.7
8	30.9	5.08	524	0.085	−0.320	2.6	1.0
9	30.5	5.68	511	0.080	−0.159	4.7	2.8
			$Re_\theta = 2.34 \times 10^4$ (two-dimensional) and 2.32×10^4 (three-dimensional)[c]				
Two-dimensional	31.3	15.8	543	——	——	——	——
0	31.0	N/A	532	N/A	N/A	N/A	N/A
1	29.3	22.8	470	0.049	0.100	−10.8	−2.2
2	28.7	18.4	451	−0.049	0.168	−23.1	−4.7
3	29.0	16.8	462	−0.320	0.131	−31.2	−7.7
4	31.1	17.3	530	−0.391	0.020	−25.7	−8.8
5	33.0	13.7	598	−0.336	−0.159	−16.3	−8.0
6	34.7	17.2	660	−0.268	−0.317	−10.3	−5.7
7	35.5	12.9	694	0.007	−0.255	−3.8	−2.7
8	35.2	13.0	682	0.028	−0.162	4.2	0.6
9	34.3	13.5	650	0.061	−0.117	6.6	2.3

[a]Pressure gradients are in wall-shear-stress coordinates. [b]Flow data of Ölçmen and Simpson.[24] [c]Flow data of Ölçmen et al.[25]

Table 2 Some relevant boundary-layer parameters

	Location[a]		$Re_\theta = 7.3 \times 10^3$ (two-dimensional) and 5.94×10^3 (three-dimensional)[b]				$Re_\theta = 2.34 \times 10^4$ (two-dimensional) and 2.32×10^4 (three-dimensional)[c]			
Station	$x \times 10^2$, m	$z \times 10^2$, m	u, m/s	ν, m^2/s ($\times 10^5$)	τ_w, Pa	d^+	u_τ, m/s	ν, m^2/s$^\tau$ ($\times 10^5$)	τ_w, Pa	d^+
Two-dimensional	——	——	0.98	1.69	1.04	29.5	1.03	1.66	1.17	31.5
0	−11.40	−3.35	1.15	1.69	1.44	34.6	N/A	1.66	N/A	30.6
1	−8.89	−3.68	0.86	1.68	0.818	26.2	0.91	1.68	0.906	27.5
2	−5.82	−4.45	0.87	1.68	0.821	26.2	0.92	1.68	0.918	27.7
3	−3.38	−5.18	0.96	1.68	1.00	29.0	1.09	1.68	1.31	33.2
4	−1.19	−6.55	1.11	1.67	1.35	33.7	1.24	1.68	1.68	37.5
5	0.66	−7.47	1.15	1.67	1.45	34.9	1.21	1.67	1.60	36.7
6	3.02	−8.38	1.16	1.67	1.48	35.3	1.21	1.67	1.60	36.7
7	5.51	−8.97	1.20	1.67	1.58	36.5	1.30	1.67	1.88	39.8
8	9.30	−9.35	1.02	1.67	1.15	31.1	1.13	1.67	1.40	34.4
9	13.11	−9.30	1.01	1.67	1.12	30.7	1.10	1.66	1.35	33.8

[a]Locations of the measurement stations given in coordinate system with an origin and orientation identical to Fig. 1 and are the same for both Reynolds number flows.
[b]Data taken from Ölçmen and Simpson.[24]
[c]Data taken from Ölçmen et al.[25]

The pressure transducer was mounted within a housing unit designed for these experiments. The housing unit was mounted flush with the surface of the test section and supported from the floor beneath the wind tunnel. The diameter of the unit was 1.55×10^{-2} m, and the hole in the test surface was 1.65×10^{-2} m in diameter. The resulting gap between the housing unit and the test surface mechanically isolated the housing unit from the wind tunnel. This prevented tunnel vibration from contaminating the surface pressure measurements. The gap was covered with 3×10^{-5} m thick cellophane tape to provide continuity of the surface while maintaining mechanical isolation of the housing unit. The tape did not contribute to surface roughness because the thickness of the tape is smaller than the viscous sublayer ($\lesssim 2.3\nu/u_\tau$).

Another technique was used to further isolate p due to turbulence from fluctuations due to other sources. Measured pressure signals are usually contaminated by coherent, facility-related acoustic inputs and external vibration of the transducer. The noise cancellation technique used by Ölçmen and Simpson,[5] which is similar to those used by Agarwal and Simpson[17] and McGrath and Simpson,[7] was used to eliminate these effects. Noise cancellation techniques rely on the relatively small coherence of turbulence-produced p in time and space. In the present study, the signal from a single transducer was delayed by the period of a given frequency and subtracted from the original signal, canceling the contributions from coherent sources at that frequency and higher harmonics. The time delay was chosen to be identical to the bin width of the power spectrum. In this way, the coherent contributions of sound and vibration are eliminated from each spectral value.

III. Uncertainty Estimates

The experimental uncertainty for the spectral power density of surface pressure fluctuations is within ±0.7 dB including the calibration, finite bandwidth, and finite record length effects.[29] The uncertainty in p' due to the uncertainty in each spectral estimate is ±10%. The uncertainty is ±0.075 in U/u_τ, ±0.05 for W/u_τ, and ±0.029 for $\overline{v^2}/u_\tau^2$ for the lower momentum thickness Reynolds number flows.[24] The uncertainty is ±0.63 in U/u_τ, ±0.29 for W/u_τ, and ±0.11 for $\overline{v^2}/u_\tau^2$ for the higher momentum thickness Reynolds number flows.[25] The uncertainty in u_τ at measurement stations 0–7 in the lower momentum thickness Reynolds number, three-dimensional flows (given by Ailinger[23]) is ±5%. The u_τ values at all of the other measurement stations in the three-dimensional flows were calculated in Refs. 24 and 25 using a curve-fit procedure that is discussed in Secs. IV.A and IV.B. The analysis of Madden[30] shows that the curve-fit procedure yields values of u_τ that are repeatable to within ±5%.

IV. Results and Discussion

A. Two-Dimensional Flows

Relevant boundary-layer flow parameters are given in Tables 1 and 2. The velocity field measurements of the lower $Re_\theta (= 7.3 \times 10^3)$ two-dimensional boundary layer are reported by Ölçmen and Simpson[24] and of the higher $Re_\theta (= 2.34 \times 10^4)$ two-dimensional boundary layer by Ölçmen et al.[25] Figures 2 and 3 include profiles of U^+, and Figs. 4 and 5 show profiles of the $\overline{v^{+2}}$ Reynolds stress. The U^+ profiles exhibit law-of-the-wall similarity,

$$U^+ = (1/\kappa)\ell n(y^+) + C \tag{1}$$

where κ and C are constants. Ölçmen and Simpson[24] calculated u_τ in the lower-Reynolds-number flow by fitting the U data to Eq. (1) using Coles's[31] constants $\kappa = 0.41$ and $C = 5$. Ölçmen et al.[25] calculated u_τ in the higher Reynolds number flow by averaging the u_τ determined by fitting the U data to Eq. (1) using Coles's[31] constants, the u_τ determined by fitting the near-wall U data to Eq. (1) using the constants of Fernholtz et al.[32] ($\kappa = 0.4$ and $C = 5.1$), and the u_τ determined by fitting the near-wall U data to a near-wall law of the wall[33]:

$$U = ay - by^4 \tag{2}$$

where $a = u_\tau^2/\nu$.

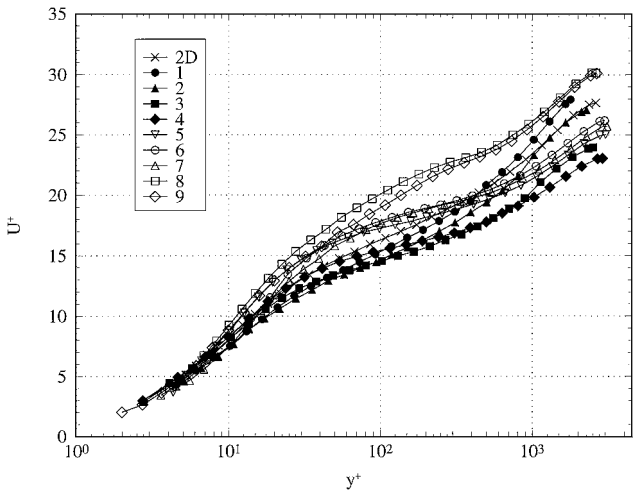

Fig. 2 U^+ mean velocity profiles in wall-shear-stress coordinates ($Re_\theta = 5.94 \times 10^3$); numbers denote measurement station (data from Ölçmen and Simpson[24]).

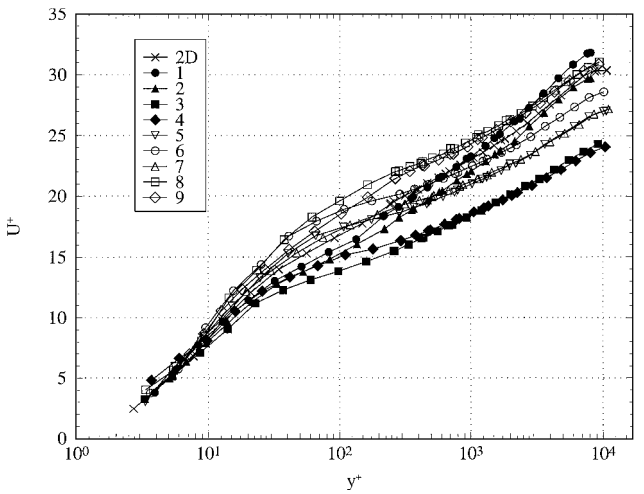

Fig. 3 U^+ mean velocity profiles in wall-shear-stress coordinates ($Re_\theta = 2.32 \times 10^4$); numbers denote measurement station (data from Ölçmen et al.[25]).

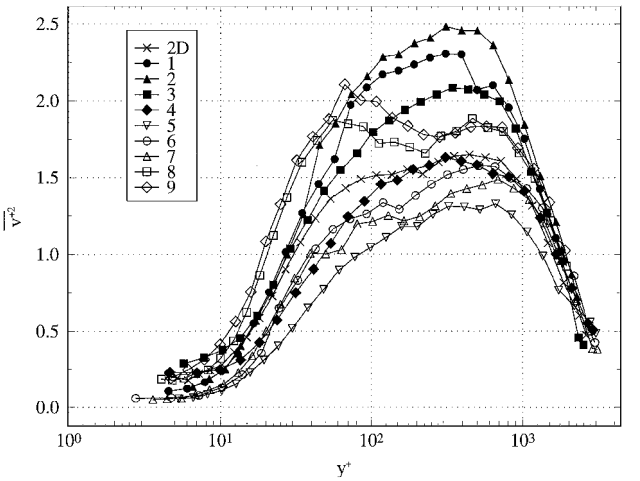

Fig. 4 Parameter $\overline{v^{+2}}$ Reynolds normal stress profiles in wall-shear-stress coordinates ($Re_\theta = 5.94 \times 10^3$); numbers denote measurement station (data from Ölçmen and Simpson[24]).

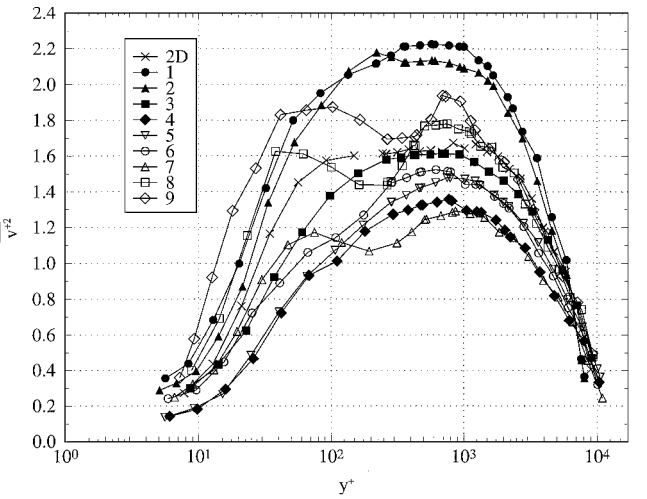

Fig. 5 Parameter $\overline{v^{+2}}$ Reynolds normal stress profiles in wall-shear-stress coordinates ($Re_\theta = 2.232 \times 10^4$); numbers denote measurement station (data from Ölçmen et al.[25]).

1. *Spectral Scaling of Surface Pressure Fluctuations*

Scaling characteristics of the power density spectrum of p show which turbulent structures are dominant for a given frequency range. For the following comparisons, the spectra presented are single sided. This required multiplying the power spectra of McGrath and Simpson,[7] Blake,[9] and Farabee and Casarella[10] by a factor of 2 (or equivalently adding 3 dB) to make them consistent with this definition. Additionally, the data of McGrath and Simpson[7] presented here is an unpublished rereduction of the original data by Shinpaugh and Simpson that corrected for the low-frequency response (< 100 Hz) of their transducer.

The high-frequency end ($\omega^+ > 0.15$) of the p spectra collapse to within measurement uncertainty when nondimensionalized using inner boundary-layer variables (ν/u_τ, u_τ, and τ_W) and agree with the earlier measurements at comparable momentum thickness Reynolds numbers (Fig. 6). This indicates that the high frequency p is due to inner layer turbulent motions near the wall. Note that no spatial resolution correction, that is, Corcos correction,[13] has been applied to the spectra presented here. The favorable comparison with other data (Fig. 6) indicate that a correction is not required. The spectra decrease as ω^{-5} for $\omega^+ > 0.8$. The high frequency ω^{-5} decay has been postulated and observed beneath two-dimensional boundary layers.[7,18]

The discrepancy between the inner-scaled spectra for $\omega^+ > 0.5$ can be attributed to transducer resolution limitations. Contributions to p from sources that are smaller than the transducer sensing

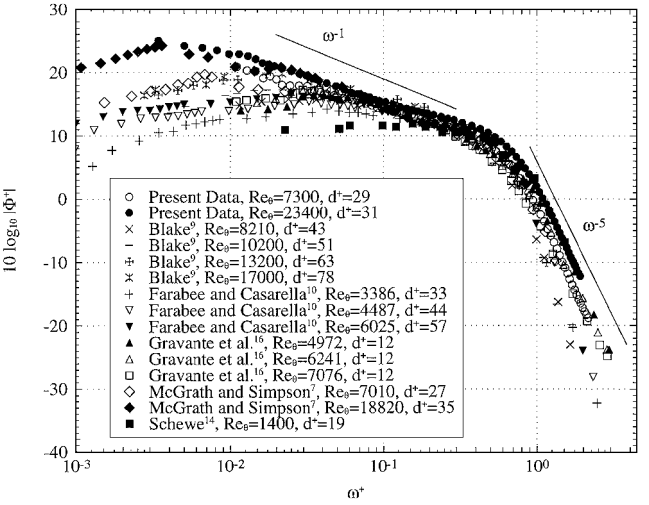

Fig. 6 Spectral power density of p beneath two-dimensional flows scaled on inner boundary-layer variables (ν/u_τ, u_τ, τ_W).

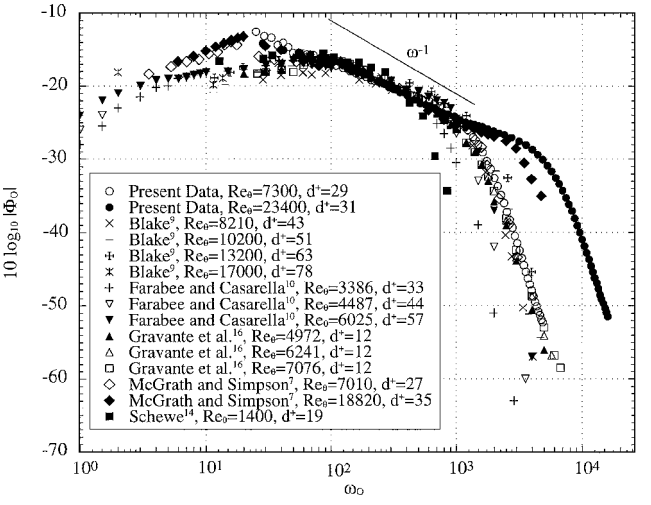

Fig. 7 Spectral power density of p beneath two-dimensional flows scaled on outer boundary-layer variables (δ, u_τ, τ_W).

area are spatially integrated and, thereby, attenuated. For $\omega^+ > 0.5$, the lower spectral values are reported by Blake[9] ($d^+ > 43$) and the higher spectral values are the present data at $Re_\theta = 2.34 \times 10^4$ ($d^+ = 31$). A lower value of d^+ indicates better transducer resolution of small-scale, high-frequency fluctuations.

There is general agreement in the literature on the proper time and pressure scales for the p spectrum at high frequencies. The same is not true for the p spectrum in the low- and middle-frequency ranges. Many researchers, such as Blake[9] and Keith et al.,[11] have used Q_e as a pressure scale and δ^*/U_e as a timescale in addition to τ_W as a pressure scale and δ^*/U_e as a timescale. Farabee and Casarella[10] and Gravante et al.[16] used τ_W as a pressure scale and δ/u_τ as a timescale.

In the present study, the p spectra for various investigations that cover a wide range of Reynolds numbers ($1.4 \times 10^3 < Re_\theta < 2.34 \times 10^4$) were made nondimensional using the length scales δ and δ^*, velocity scales u_τ and U_e, and pressure scales τ_W and Q_e. None of the eight possible scaling combinations successfully collapsed the p spectra at the lowest frequencies presented here. Note that the data of Farabee and Casarella[10] collapse using Q_e as a pressure scale and δ^*/U_e as a timescale for $\omega\delta^*/U_e < 0.03$, which is outside the frequency range of all other p spectra presented here. Within the middle-frequency range, the p spectra collapse when non-dimensionalized using τ_W to scale pressure independent of the timescale used. Figure 7 shows the p spectra scaled on τ_W and δ/u_τ as an example. The spectra collapse in the frequency range $100 < \omega_0 < 500$, which is the lower end of the overlap range of Farabee and Casarella.[10]

It has been postulated,[6,8,18,34] using arguments relating the existence of an inner scaling and an outer scaling, that an overlap region exists in the p spectrum beneath two-dimensional boundary layers at high Reynolds number. Both an inner and an outer boundary-layer scaling collapse the power spectrum in the overlap region. (The theoretical arguments that support the existence of an overlap region require specific forms for the inner- and outer-scaling laws. See Refs. 6, 8, 18, and 34 for further discussion of this issue.) Bradshaw[6] argued that the p spectrum in this region decreases as ω^{-1} and is due to universal turbulent motions within the log layer where the convection velocity approaches the local mean velocity. The size/existence of this region increases as boundary-layer thickness Reynolds number increases and is related to Kolmogorov's hypothesis[35] of an energy cascade.

The p spectrum for the higher momentum thickness Reynolds number flows ($Re_\theta > 1.88 \times 10^4$) exhibit an overlap region. For the present data at $Re = 2.34 \times 10^4$ the frequency range $0.03 < \omega^+ < 0.06$ corresponds to $250 < \omega_0 < 500$. Examination of Figs. 6 and 7 reveals that both scalings collapse the p spectra and follow a power law decay within this range. An ω^{-1} decay is included in Figs. 6 and 7 because it has a theoretical basis. However, the observed spectral decay is closer to $\omega^{-0.8}$. Blake[9] observed an $\omega^{-0.75}$ decay, and

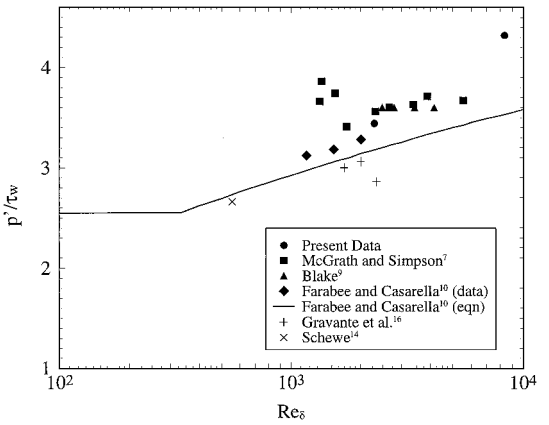

Fig. 8 Root mean square of p as a function of Reynolds number based on boundary-layer thickness.

McGrath and Simpson[7] observed an $\omega^{-0.7}$ decay within the overlap region. Note that exact slopes are difficult to measure. Also notable is that the size of the middle-frequency range in which the p spectra exhibit a power law decay increases with Reynolds number. The low $Re_\theta (= 1.4 \times 10^3)$ p data of Schewe[14] only tangentially approach a power law decay whereas the high $Re_\theta (= 2.34 \times 10^4)$ p data of the present study exhibit a power law decay for $30 < \omega_0 < 2000$.

2. Root Mean Square of Surface Pressure Fluctuations

Each of the p spectra was integrated to obtain $\overline{p^2}$ values. Figure 8 shows p'/τ_W as a function of boundary-layer thickness Reynolds number. Although there is scatter in p'/τ_W values due to transducer resolution limitations and accumulated experimental errors in individual frequency-spectral values, there is a general trend of increasing p'/τ_W with boundary-layer thickness Reynolds number. Previous investigations[6,8,10,12] have found that p'/τ_W increases logarithmically with Reynolds number. Farabee and Casarella[10] propose an equation for $\overline{p^2}/\tau_W^2$ (solid line in Fig. 8):

$$\frac{\overline{p^2}}{\tau_W^2} = \begin{cases} 6.5 & (Re_\delta \le 333) \\ 6.5 + 1.86\,\ell n(Re_\delta/333) & (Re_\delta > 333) \end{cases} \qquad (3)$$

by numerically integrating their measured spectra and accounting for the Reynolds number dependence of the overlap region. The trend shown in Fig. 8 is consistent with a logarithmic increase in p'/τ_w with Reynolds number; however, the level proposed by Farabee and Casarella[10] is lower than most of the data shown in Fig. 8.

Table 3 Variation of $\overline{p^2}$ and p' for the lower Reynolds number flows and low- and high-frequency contributions to the $\overline{p^2}$ integral[a]

Station	$\overline{p^2}$, Pa^2	Contribution to $\overline{p^2}$ integral, Pa^2				p'/τ_W	p'/Q_e	$\overline{p^2}$, Pa^2	Nonflat
		<1 kHz		>1 kHz					
$Re_\theta = 7.3 \times 10^3$ (two-dimensional) and 5.94×10^3 (three-dimensional)									
Two-dimensional	12.9	5.4	42%	7.5	58%	3.44	0.0090	——	——
0	13.7	7.3	53%	6.4	47%	2.57	0.0098	——	——
1	14.8	8.3	56%	6.5	44%	4.71	0.0114	——	——
2	17.5	10.8	62%	6.7	38%	5.10	0.0124	——	——
3	21.4	14.7	69%	6.7	31%	4.61	0.0132	——	——
4	27.7	13.1	47%	14.6	53%	3.90	0.0129	21.9	79%
5	17.6	10.1	57%	7.5	43%	2.89	0.0088	15.8	90%
6	20.7	8.2	40%	12.5	60%	3.08	0.0089	17.1	82%
7	28.7	8.1	28%	20.6	72%	3.39	0.0102	20.2	70%
8	30.6	7.9	26%	22.7	74%	4.80	0.0106	23.2	76%
9	33.0	9.5	29%	23.5	71%	5.12	0.0113	23.2	70%
$Re_\theta = 2.34 \times 10^4$ (two-dimensional) and 2.32×10^4 (three-dimensional)									
Two-dimensional	25.8	11.4	44%	14.4	56%	4.32	0.0094	——	——
0	26.8	15.4	57%	11.4	43%	4.67	0.0097	——	——
1	27.8	17.3	62%	10.5	38%	5.81	0.0112	——	——
2	33.8	23.6	70%	10.2	30%	6.34	0.0129	——	——
3	40.1	30.2	75%	9.9	25%	4.82	0.0137	——	——
4	34.2	24.6	72%	9.6	28%	3.48	0.0110	——	——
5	29.5	18.7	63%	10.8	37%	3.39	0.0091	26.2	89%
6	30.2	15.2	50%	15.0	50%	3.43	0.0083	23.3	77%
7	36.1	13.6	38%	22.5	62%	3.20	0.0087	24.2	67%
8	38.8	12.6	32%	26.2	68%	4.44	0.0091	23.3	60%
9	41.3	13.2	32%	28.1	68%	4.77	0.0099	28.3	68%

[a] Values of $\overline{p^2}$ calculated by integrating the p spectra.

B. Three-Dimensional Flows

The complexity of the skewed three-dimensional boundary layer (Fig. 1) necessitates the use of multiple coordinate systems. The tunnel coordinate system is right handed with the x axis parallel to the tunnel centerline pointing downstream and the y axis perpendicular to the tunnel floor pointing up. The wall-shear-stress coordinate system is right handed with the x axis in the shear-stress direction at the wall as approximated by the measured mean-flow angle closest to the wall.[1,26,27] The y axis is normal to the wall, pointing up. Details of the velocity field are given in the following sections as they relate to p. Discussion of the velocity field alone may be found elsewhere.[1,23–27]

Relevant boundary-layer flow parameters are given in Tables 1 and 2. The velocity measurements of the lower $Re_\theta (=5.94 \times 10^3)$ boundary layer are reported by Ölçmen and Simpson[24] and of the higher $Re_\theta (=2.32 \times 10^4)$ boundary layer by Ölçmen et al.[25] The u_τ at measurement stations 0–7 in the lower momentum thickness Reynolds number boundary layer were measured by Ailinger[23] using oil-film interferometry. The u_τ at measurement stations 8 and 9 in the lower momentum thickness Reynolds number boundary layer were calculated by Ölçmen and Simpson[24] by fitting the near-wall U data in wall-shear-stress coordinates to a near-wall law of the wall [Eq. (2)]. The u_τ at all of measurement stations in the higher momentum thickness Reynolds number boundary layer were calculated by Ölçmen et al.[25] by fitting the near-wall U data in wall-shear-stress coordinates to a near-wall law of the wall [Eq. (2)].

1. Root Mean Square of Surface Pressure Fluctuations and Features of the Velocity Field

Each of the p spectra was integrated to obtain the $\overline{p^2}$ values given in Table 3. For the lower momentum thickness Reynolds number flow (Table 3) p'/τ_W and p'/Q_e beneath the three-dimensional flows are higher than beneath the two-dimensional flow and increase with station number for stations 0–3 due to adverse pressure gradient effects on the lower frequencies.[36] Also Table 3 indicates that most of the p' is due to low-frequency ($f < 1$ kHz) fluctuations, which increase in magnitude with station number. The $\overline{p^2}$ from low frequencies at station 3 is double the low frequency $\overline{p^2}$ at station 0. The high-frequency ($f > 1$ kHz) contribution to p' at stations 0–3 is nearly constant.

The lateral pressure gradient in wall-shear-stress coordinates (Table 1) pushes the flow away from the wing at stations 0–3. Ölçmen and Simpson[24] report that at stations 0–3 the mean flow angle changes monotonically from near the wall to the freestream by $4.4 < |\beta_{FS} - \beta_W| < 25$ deg (Fig. 1). Examination of Table 3 and the dimensional p spectra (Figs. 9 and 10) suggest that the montonic (in y) turning of the mean flow at stations 0–3 has little effect on high-frequency p (which have a lower spectral level than the two-dimensional at comparable momentum thickness Reynolds number, but increase the low frequency p substantially.

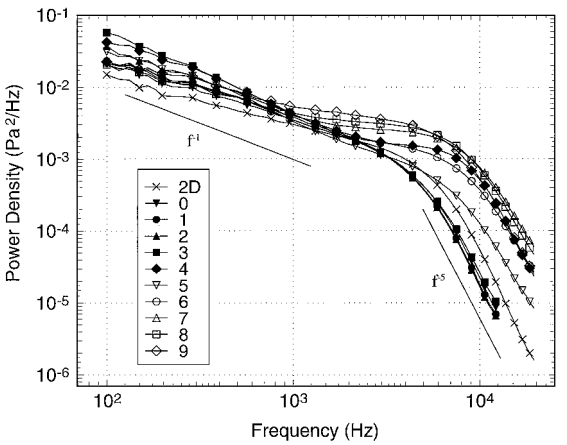

Fig. 9 Spectral power density of p [$Re_\theta = 7.3 \times 10^3$ (two dimensional) and 5.94×10^3 (three-dimensional)]; numbers denote measurement station in three-dimensional flow.

The lateral pressure gradient in wall-shear-stress coordinates (Table 1) changes sign between stations 3 and 4. At stations 4–9 the lateral pressure gradient pushes the mean flow back toward the wing. Ölçmen and Simpson[24] (page 7) observed that "At station 4 the W/u_τ values are close to zero up to $y^+ \approx 40$. Above this y location, values montonically increase. At stations farther downstream the effect of the sign change of the lateral pressure gradient is felt most near the wall. This results in negative W/u_τ values.... The pressure force is most effective on the near-wall flow where the momentum of the flow is lowest." Figures 11 and 12 show the W/u_τ mean velocity profiles in wall-shear-stress coordinates. Note that the location of maximum W propagates outward from the wall at successive downstream stations.[24,25]

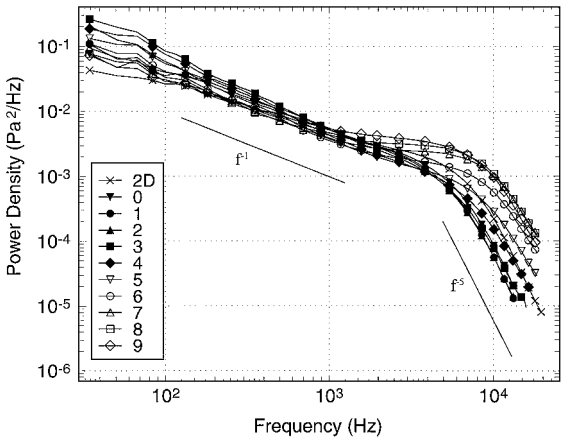

Fig. 10 Spectral power density of p[$Re_\theta = 2.34 \times 10^4$ (two-dimensional) and 2.32×10^4 (three-dimensional)]; numbers denote measurement station in the three-dimensional flow.

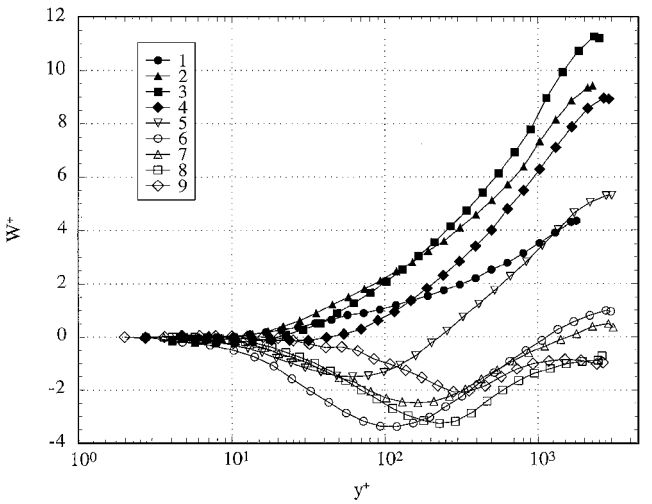

Fig. 11 W^+ mean velocity profiles in wall-shear-stress coordinates ($Re_\theta = 5.94 \times 10^3$); numbers denote measurement station (data from Ölçmen and Simpson[24]).

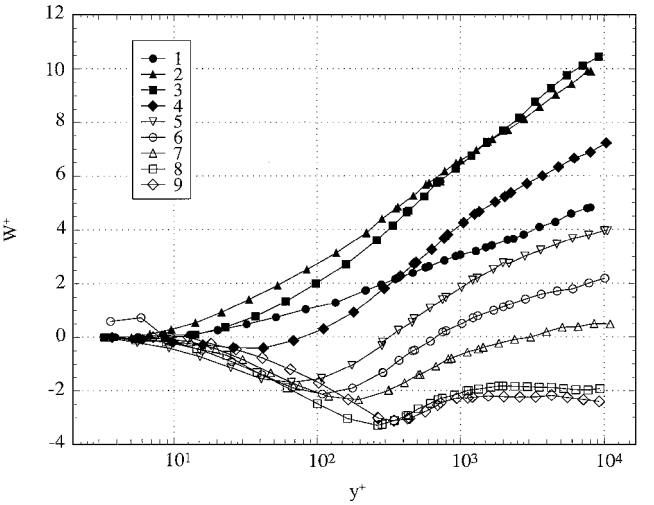

Fig. 12 W^+ mean velocity profiles in wall-shear-stress coordinates ($Re_\theta = 2.32 \times 10^4$); numbers denote measurement station (data from Ölçmen et al.[25]).

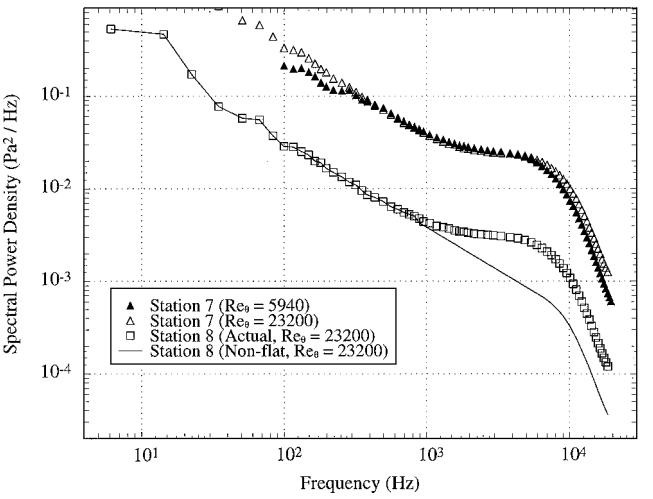

Fig. 13 Spectral power density of p at stations 7 and 8; station 7 data are multiplied by 10 for clarity.

For stations 4–8 the mean velocity at the boundary-layer edge accelerates (Table 1). The magnitude displacement thickness δ^* decreases as well as the $\overline{p^2}$ contribution from low-frequency fluctuations ($f < 1$ kHz) (Table 3). Whereas the details of the preceding $\overline{p^2}$ discussion is confined to the $Re_\theta = 5.94 \times 10^3$ flow, similar trends are present in the $Re_\theta = 2.32 \times 10^4$ data.

2. Features of the Dimensional Power Spectra

The most significant feature of the spectral power density spectrum of surface pressure fluctuations (Figs. 9 and 10) at stations 4–9 is the constant (or nearly constant) spectral levels in the frequency range $2 < f < 5$ kHz. A flat midfrequency spectral region has been previously observed in the three-dimensional flow on the leeside of a prolate spheroid at angle of attack.[37] Goody et al.[37] attributed the flat-midfrequency spectral region to the lack of overlapping frequency structure between the large-scale motions of the outer layer and the viscous-dominated near-wall region. A similar situation exists in the present study. The lateral pressure gradient imposed by the presence of the wing skews the the near-wall, low momemtum mean flow. The larger near-wall velocity gradients associated with the skewed flow produces high-frequency pressure fluctuations as prescribed by the Poisson integral.[18]

The effect of the flat spectral region on $\overline{p^2}$ is significant. Table 3 shows the effect on $\overline{p^2}$ of removing the spectral contribution that makes the region flat. Figure 13 shows the p spectrum at station 8, $Re_\theta = 2.32 \times 10^4$ as an example. At station 8, the flat spectral region accounts for 40% of the $\overline{p^2}$ integral (Table 3). The nonflat spectrum shown in Fig. 13 was determined by extending the power law decay of the spectrum at frequencies below the flat region and tacking on the high-frequency spectral variation at the end. Details are given by Goody.[38]

The physical mechanism that produces the flat spectral region appears to be independent of, or at least slowly varying with, Reynolds number. As station number increases from 0 to 3, the p spectral level beneath the lower momentum thickness Reynolds number flow approaches the p spectral level beneath the higher momentum thickness Reynolds number flow at middle frequencies. The p spectra generally overlap at stations 4–9 for 300 Hz $< f <$ 3 kHz. An example of this is station 7 (Fig. 13) where the overlap extends to 7 kHz. Ölçmen et al.[27] discuss Reynolds number effects for the flows studied here. They found that, although the magnitude of the shear stresses (normalized on u_τ) increases with Reynolds number, below $y^+ = 100$ the stresses tend to overlap.

3. Spectral Scaling of Surface Pressure Fluctuations

The p spectra at the three-dimensional stations do not collapse when made nondimensional using boundary-layer parameters that collapse the p spectra in two-dimensional flows. The lack of scaling parameters that collapse the p spectra is not surprising given the complexity of these three-dimensional flows. In two-dimensional equilibrium boundary layers, similarity parameters exist that scale the velocity, for example, law of the wall and defect law. In the three-dimensional flows of the present study, the only scaling that

collapses any part of the velocity profile is $U^+ = y^+$ near the wall ($y^+ < 5$), when the velocity is expressed in wall-shear-stress coordinates. Additionally, the frequency/wave number dependence of the wave speed of p is exacerbated in this three-dimensional flow because turbulent structures travel in different directions depending on the distance from the wall.[28] To be successful, scaling parameters for p beneath three-dimensional flows must incorporate more detailed velocity field information through the Poisson equation.

Previous analysis of two-dimensional flows[6,8,18] have shown that the Poisson integral is dominated by the mean-shear-turbulence term in the form

$$p \approx \frac{\rho}{\pi} \oint_{\Omega} \left[\frac{\partial U}{\partial y} \frac{\partial v}{\partial x} \right] \frac{d\Omega}{r_S} \tag{4}$$

For the present flow, it is assumed that the high frequency p is generated by small-scale velocity fluctuations near the wall. In a study of three-dimensional turbulent boundary layers, Ölçmen and Simpson[39] showed that the near-wall region of the mean velocity profile follows a two-dimensional wall law reasonably well. Therefore, it is assumed here that, as with two-dimensional boundary layers, high-frequency contributions to the Poisson integral are dominated by the mean-shear-turbulence term and that derivatives of the mean velocity in the x and z direction are negligible. Because the y derivative of the W component of velocity is not always negligible in the present flow, the two-dimensional approximation of the Poisson integral [Eq. (4)] is modified in the form

$$p \approx \frac{\rho}{\pi} \oint_{\Omega} \left[\frac{\partial U}{\partial y} \frac{\partial v}{\partial x} + \frac{\partial W}{\partial y} \frac{\partial v}{\partial z} \right] \frac{d\Omega}{r_S} \tag{5}$$

Consider the variation of Eq. (5) from station to station with the goal of describing the high-frequency end of the p spectra beneath the three-dimensional flows of the present study.

Some simplifying assumptions must be made to evaluate Eq. (5) with the data available. It is assumed that the small-scale turbulent structures near the wall are homogenous in planes parallel to the wall and behave as traveling waves, which is similar to a recent model for the p spectrum under a three-dimensional boundary layer that was proposed by Panton.[21] Therefore, $v = v_\omega \cos(\omega t - k_1 x - k_3 z)$, where v_ω is v at a particular frequency and $k_1 = \omega / U_{c1}$ and $k_3 = \omega / U_{c3}$ are the wave numbers in the x and z directions, respectively. The traveling wave model results in

$$\frac{\partial v}{\partial x} = k_1 v_\omega \sin(\omega t - k_1 x - k_3 z), \quad \text{which varies like} \quad k_1 v_\omega$$

$$\frac{\partial v}{\partial z} = k_3 v_\omega \sin(\omega t - k_1 x - k_3 z), \quad \text{which varies like} \quad k_3 v_\omega \tag{6}$$

High-frequency contributions to the p spectrum primarily originate in the near-wall region, where the flow closely scales on the wall variables ν/u_τ and u_τ. Rewriting Eq. (5) with these considerations in mind results in

$$\frac{p}{\tau_W} \approx \frac{1}{\pi} \oint_{\Omega^+} \left(k_1^+ v_\omega^+ \frac{\partial U^+}{\partial y^+} + k_3^+ v_\omega^+ \frac{\partial W^+}{\partial y^+} \right) \frac{d\Omega^+}{r_S^+} \tag{7}$$

Because near-wall turbulent structures have small spatial extent and in light of the $1/r_S^+$ dependence of Eq. (7), it is assumed that the variation of p/τ_W at a particular high frequency results mainly from the variation of the integrand of Eq. (7). Furthermore, the variation of the integrand of Eq. (7) at a particular wave number (or frequency) may be approximated by the variation of $\overline{v^+}(\partial U^+/\partial y^+ + \partial W^+/\partial y^+)$ at a particular distance from the wall. Figures 11 and 12 show the variation of $\partial W^+/\partial y^+$ in wall-shear-stress coordinates near the wall from station to station. Figures 2 and 3 show the variation of $\partial U^+/\partial y^+$ and Figs. 4 and 5 show the variation of $\overline{v^{+2}}$ in wall-shear-stress coordinates near the wall from station to station.

Modification of the inner variable scaling shown in Figs. 14a and 15a is required to account for the variation of the Poisson integrand [approximated by $\overline{v^+}(\partial U^+/\partial y^+ + \partial W^+/\partial y^+)$] near the wall from station to station. With the knowledge that each spectral value of

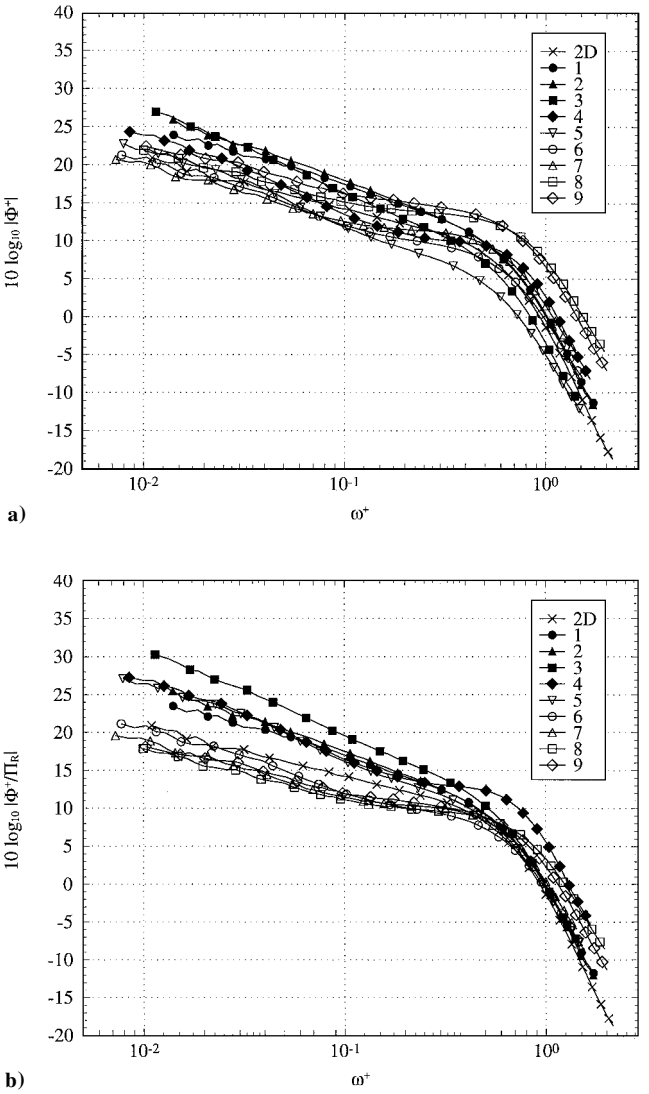

Fig. 14 Nondimensional p spectra [$Re_\theta = 7.3 \times 10^3$ (two-dimensional) and 5.94×10^3 (three-dimensional)]; numbers denote measurement station in three-dimensional flow: a) scaled on inner boundary-layer variables (ν/u_τ, u_τ, τ_W) alone and b) scaled using inner boundary-layer variables and Poisson equation term ratio evaluated at $y^+ = 50$.

the p spectrum is the contribution of p within a narrow frequency band to $\overline{p^2}$, a Poisson equation term ratio Π_R is formed as

$$\Pi_R = \left[\frac{\overline{p^2}}{\tau_W^2} \right]_{3\text{-}D} \Bigg/ \left[\frac{\overline{p^2}}{\tau_W^2} \right]_{2\text{-}D}$$

$$= \left[\overline{v^{+2}} \left(\frac{\partial U^+}{\partial y^+} + \frac{\partial W^+}{\partial y^+} \right)^2 \right]_{3\text{-}D} \Bigg/ \left[\overline{v^{+2}} \left(\frac{\partial U^+}{\partial y^+} \right)^2 \right]_{2\text{-}D} \tag{8}$$

The wall-shear-stress coordinate system was used because it is aligned with the near-wall flow. Therefore, phase errors that are introduced by the approximations of the turbulent velocity structure in the x and z directions are minimized. Also, a spectral ratio Φ_R of $\Phi^+(\omega^+ = 1)$ at each measurement station in the three-dimensional flow to $\Phi^+(\omega^+ = 1)$ in the two-dimensional flow at comparable momentum thickness Reynolds number is used as a measure of the variation of the high-frequency pressure spectral levels. By evaluating Π_R at various near-wall y^+ locations, the change in Π_R closely tracked the change in Φ_R from station to station. An example is shown in Figs. 14b and 15b, where Π_R is evaluated at $y^+ = 50$. Figures 14 and 15 show that the variation of the high-frequency spectra in the present nonequilibrium three-dimensional flows result from features of the near-wall velocity field that change Π_R from station to station. It is also significant that the complex variations in the

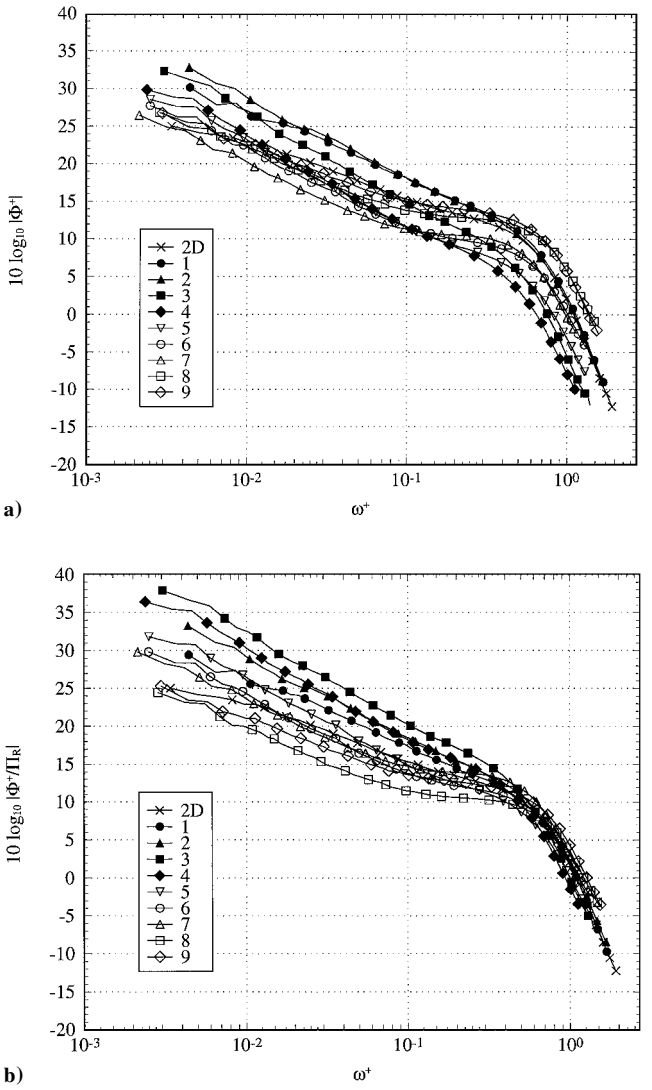

Fig. 15 Nondimensional p spectra [$Re_\theta = 2.34 \times 10^4$ (two-dimensional) and 2.32×10^4 (three-dimensional)]; numbers denote measurement station in three-dimensional flow: a) scaled on inner boundary-layer variables (ν/u_τ, u_τ, τ_W) alone and b) scaled using inner boundary-layer variables and Poisson equation term ratio evaluated at $y^+ = 50$.

high-frequency pressure spectrum are tracked by a relatively simple term, Π_R, which only requires mean velocity and Reynolds stress data.

V. Conclusions

Surface pressure fluctuation measurements beneath two Reynolds number two-dimensional turbulent boundary layers and high-Reynolds-number three-dimensional boundary layers were presented. For the two-dimensional flows the p spectra collapse within the frequency range $100 < \omega_0 < 500$ when scaled on outer boundary-layer variables and collapse at high frequencies ($\omega^+ > 0.15$) when scaled on inner boundary-layer variables. Additionally, both scalings collapse the p spectra within a midfrequency range. The size of the frequency range of spectral overlap increases with Reynolds number. The two-dimensional scaling behavior shown holds for for a large range of Reynolds number ($1.4 \times 10^3 < Re_\theta < 2.34 \times 10^4$) and is consistent with other researchers.

Scaling parameters that collapse the pressure spectra beneath two-dimensional flows do not collapse the pressure spectra beneath three-dimensional flows. The flows decelerate at stations upstream of the wing, which increases the magnitude of low frequency p significantly, but has little effect on the high frequency p. The flow turns and accelerates at stations to the side of the wing, which decreases the magnitude of low frequency p and increases the magnitude of high frequency p. Spectral levels of p at these stations are nearly constant and do not change appreciably with Reynolds number within a middle-frequency range. A flat-midfrequency spectral region has been previously observed in the three-dimensional flow on the leeside of a prolate spheroid at angle of attack.[37] Analysis based on the Poisson equation shows that the variation of high frequency p is tracked by the variation of mean velocity gradients and $\overline{v^2}$ structure near the wall. The increased spectral levels at high frequencies increase p' significantly. Therefore, accurate measurement of p' requires the accurate measurement of high frequency p particularly when large changes in near-wall mean velocity gradients and $\overline{v^2}$ structure are present.

Acknowledgments

The authors appreciate the support of the Office of Naval Research under Grant N00014-94-1-0092 and Grant N00014-94-1-0802, L. P. Purtell, Program Manager.

References

[1]Ölçmen, M. S., and Simpson, R. L., "An Experimental Study of a Three-Dimensional Pressure-Driven Turbulent Boundary Layer," *Journal of Fluid Mechanics*, Vol. 290, 1995, pp. 225–262.

[2]Simpson, R. L., "Aspects of Turbulent Boundary-Layer Separation," *Progress in Aerospace Sciences*, Vol. 32, Pergamon, Oxford, 1996, pp. 457–521.

[3]Fleming, J. L., and Simpson, R. L., "Experimental Investigation of the Near Wall Flow Structure of a Low Reynolds Number 3-D Turbulent Boundary Layer," Dept. of Aerospace and Ocean Engineering, Data Rept. VPI-AOE-247, Virginia Polytechnic Inst. and State Univ., Blacksburg, VA, April 1997.

[4]Rife, M. C., Devenport, W. J., and Simpson, R. L., "An Experimental Study of the Relationship Between Velocity and Pressure Fluctuations in a Wing-Body Junction," Dept. of Aerospace and Ocean Engineering, Data Rept. VPI-AOE-188, Virginia Polytechnic Inst. and State Univ., Blacksburg, VA, Jan. 1992.

[5]Ölçmen, M. S., and Simpson, R. L., "Influence of Wing Shapes on Surface Pressure Fluctuations at Wing–Body Junctions," *AIAA Journal*, Vol. 32, No. 1, 1994, pp. 6–15.

[6]Bradshaw, P., "Inactive Motion and Pressure Fluctuations in Turbulent Boundary Layers," *Journal of Fluid Mechanics*, Vol. 30, Pt. 2, 1967, pp. 241–258.

[7]McGrath, B. E., and Simpson, R. L., "Some Features of Surface Pressure Fluctuations in Turbulent Boundary Layers with Zero and Favorable Pressure Gradients," NASA CR-4051, 1987.

[8]Panton, R. L., and Linebarger, J. H., "Wall Pressure Spectra Calculations for Equilibrium Boundary Layers," *Journal of Fluid Mechanics*, Vol. 65, Pt. 2, 1974, pp. 261–287.

[9]Blake, W. K., "Turbulent Boundary-Layer Wall-Pressure Fluctuations on Smooth and Rough Walls," *Journal of Fluid Mechanics*, Vol. 44, Pt. 4, 1970, pp. 637–660.

[10]Farabee, T. M., and Casarella, M. J., "Spectral Features of Wall Pressure Fluctuations Beneath Turbulent Boundary Layers," *Physics of Fluids A*, Vol. 3, No. 10, 1991, pp. 2410–2420.

[11]Keith, W. L., Hurdis, D. A., and Abraham, B. M., "A Comparison of Turbulent Boundary Layer Wall-Pressure Spectra," *Journal of Fluids Engineering*, Vol. 114, No. 2, 1992, pp. 338–347.

[12]Bull, M. K., "Wall-Pressure Fluctuations Beneath Turbulent Boundary Layers: Some Reflections on Forty Years of Research," *Journal of Sound and Vibration*, Vol. 190, No. 3, 1996, pp. 299–315.

[13]Corcos, G. M., "Resolution of Pressure in Turbulence," *Journal of the Acoustical Society of America*, Vol. 35, No. 2, 1963, pp. 192–199.

[14]Schewe, G., "On the Structure and Resolution of Wall-Pressure Fluctuations Associated with Turbulent Boundary Layer Flow," *Journal of Fluid Mechanics*, Vol. 134, 1983, pp. 311–328.

[15]Lueptow, R. M., "Transducer Resolution and the Turbulent Wall Pressure Spectrum," *Journal of the Acoustical Society of America*, Vol. 97, No. 1, 1995, pp. 370–378.

[16]Gravante, S. P., Naguib, A. M., Wark, C. E., and Nagib, H. M., "Characterization of the Pressure Fluctuations Under a Fully Developed Turbulent Boundary Layer," *AIAA Journal*, Vol. 36, No. 10, 1998, pp. 1808–1816.

[17]Agarwal, N. K., and Simpson, R. L., "A New Technique for Obtaining the Turbulent Pressure Spectrum from the Surface Pressure Spectrum," *Journal of Sound and Vibration*, Vol. 135, No. 2, 1989, pp. 346–350.

[18]Blake, W. K., *Mechanics of Flow-Induced Sound and Vibration*, Academic Press, New York, 1986, pp. 497–595.

[19]Kraichnan, R. H., "Pressure Fluctuations in Turbulent Flow over a Flat Plate," *Journal of the Acoustical Society of America*, Vol. 28, No. 3, 1956, pp. 378–390.

[20]Rotta, J. C., "Turbulent Boundary Layers in Incompressible Flow," *Progress in Aeronautical Sciences*, Vol. 2, Pergamon, Oxford, 1962, pp. 10, 11.

[21]Panton, R. L., "On the Wall-Pressure Spectrum Under a Three-Dimensional Boundary Layer," *Journal of Fluids Engineering*, Vol. 120, No. 2, 1998, pp. 407–410.

[22]Witting, J., M., "A Spectral Model of Pressure Fluctuations at a Rigid Wall Bounding an Incompressible Fluid, Based on Turbulent Structures in the Boundary Layer," *Noise Control Engineering Journal*, Vol. 26, No. 1, 1986, pp. 28–43.

[23]Ailinger, K., "Measurements of Surface Shear Stresses Under a Three-Dimensional Turbulent Boundary Layer Using Oil-Film Interferometry," M.S. Thesis, Dept. of Aerospace and Ocean Engineering, Virginia Polytechnic Inst. and State Univ., Blacksburg, VA, Aug. 1990.

[24]Ölçmen, M. S., and Simpson, R. L., "Higher Order Turbulence Results for a Three-Dimensional Pressure-Driven Turbulent Boundary Layer," Dept. of Aerospace and Ocean Engineering, Data Rept. VPI-AOE-237, Virginia Polytechnic Inst. and State Univ., Blacksburg, VA, 1996.

[25]Ölçmen, M. S., Simpson, R. L., George, J., and Whitfield, C., "Experimental Study of High Reynolds Number (Re = 23000) Two- and Three-Dimensional Turbulent Boundary Layers," Dept. of Aerospace and Ocean Engineering, Data Rept. VPI-AOE-260, Virginia Polytechnic Inst. and State Univ., Blacksburg, VA, 1998.

[26]Ölçmen, M. S., Simpson, R. L., and George, J., "Experimental Study of High Reynolds Number (Re_θ = 23200) Two- and Three-Dimensional Turbulent Boundary Layers," AIAA Paper 99-0553, Jan. 1999.

[27]Ölçmen, M. S., Simpson, R. L., and George, J., "Some Reynolds Number Effects on a Three-Dimensional Turbulent Boundary Layer," AIAA Paper 99-0554, Jan. 1999.

[28]Ha, S. M., and Simpson, R. L., "An Experimental Study of Coherent Structures in a Three-Dimensional Turbulent Boundary Layer," Dept. of Aerospace and Ocean Engineering, Data Rept. VPI-AOE-205, Virginia Polytechnic Inst. and State Univ., Blacksburg, VA, 1993.

[29]Bendat, J. S., and Piersol, A. G., *Random Data: Analysis and Measurement*, 2nd ed., Wiley, New York, 1986, pp. 252–290.

[30]Madden, M. M., "Octant Analysis of the Reynolds Stresses in the Three-Dimensional Turbulent Boundary Layer of a Prolate Spheroid," M.S. Thesis, Dept. of Aerospace and Ocean Engineering, Virginia Polytechnic Inst. and State Univ., Blacksburg, VA, 1997.

[31]Coles, D., "The Law of the Wake in the Turbulent Boundary Layer," *Journal of Fluid Mechanics*, Vol. 1, Pt. 2, 1956, pp. 191–226.

[32]Fernholtz, H. H., Krause, E., Nockemann, M., and Schober, M., "Comparative Measurement in the Canonical Boundary Layer at $Re_\theta \leq 6 \times 10^4$ on the Wall of the German–Dutch Wind Tunnel," *Physics of Fluids*, Vol. 7, No. 6, 1995, pp. 1275–1281.

[33]Spalding, D. B., "A Single Formula for the Law of the Wall," *Conference on Internal Developments in Heat Transfer*, Pt. 2, American Society of Mechanical Engineers, Fairfield, NJ, 1961, pp. 439–446.

[34]Panton, R. L., "Small Silicon Pressure Transducers for Space-Time Correlation Measurements in a Flat Plate Boundary Layer" (comment on Lofdahl, L., Kalveston, E., and Stemme, G., Vol. 118, Sept. 1996, pp. 457–463), *Journal of Fluids Engineering*, Vol. 118, No. 4, pp. 879–880.

[35]Tennekes, H., and Lumley, J. L., *A First Course in Turbulence*, MIT Press, Cambridge, MA, 1972, pp. 260–267.

[36]Simpson, R. L., Ghodbane, M., and McGrath, B. E., "Surface Pressure Fluctuations in a Separating Turbulent Boundary Layer," *Journal of Fluid Mechanics*, Vol. 177, 1987, pp. 167–186.

[37]Goody, M. C., Simpson, R. L., and Chesnakas, C. J., "Surface Pressure Fluctuations and Pressure–Velocity Correlations Produced by a Separated Flow Around a Prolate Spheroid at Incidence," *AIAA Journal*, Vol. 38, No. 2, 2000, pp. 266–274.

[38]Goody, M. C., "An Experimental Investigation of Pressure Fluctuations in Three-Dimensional Turbulent Boundary Layers," Ph.D. Dissertation, Dept. of Aerospace and Ocean Engineering, Virginia Polytechnic Inst. and State Univ., Blacksburg, VA, Dec. 1999.

[39]Ölçmen, M. S., and Simpson, R. L., "Perspective: On the Near Wall Similarity of Three-Dimensional Turbulent Boundary Layers," *Journal of Fluids Engineering*, Vol. 114, No. 4, 1992, pp. 487–495.

M. Samimy
Associate Editor